Mechanics of Advanced Materials and Structures

ISSN: 1537-6494 (Print) 1537-6532 (Online) Journal homepage: www.tandfonline.com/journals/umcm20

Active vibration control of high-stiffness heavy cantilever beam based on piezoelectric stack actuators

Jianlong Gao, Pengxiang Zhao, Xudong Zhang, Weikai Shi, Yaxiang Sun, Xin Lan, Yanju Liu & Jinsong Leng

To cite this article: Jianlong Gao, Pengxiang Zhao, Xudong Zhang, Weikai Shi, Yaxiang Sun, Xin Lan, Yanju Liu & Jinsong Leng (2026) Active vibration control of high-stiffness heavy cantilever beam based on piezoelectric stack actuators, Mechanics of Advanced Materials and Structures, 33:1, 2468375, DOI: 10.1080/15376494.2025.2468375

To link to this article: https://doi.org/10.1080/15376494.2025.2468375

MECHANICS OF ADVANCED MATERIALS AND STRUCTURES
2026, VOL. 33, NO. 1, 2468375
https://doi.org/10.1080/15376494.2025.2468375

Taylor & Francis
Taylor & Francis Group

ORIGINAL ARTICLE

Active vibration control of high-stiffness heavy cantilever beam based on piezoelectric stack actuators

Jianlong Gao[a], Pengxiang Zhao[a], Xudong Zhang[a], Weikai Shi[a], Yaxiang Sun[b], Xin Lan[b], Yanju Liu[a], and Jinsong Leng[b]

[a]Department of Astronautical Science and Mechanics, Harbin Institute of Technology, Harbin, People's Republic of China; [b]Centre for Composite Materials and Structures, Harbin Institute of Technology, Harbin, People's Republic of China

ABSTRACT

Piezoelectric materials are utilized in active vibration control (AVC) because of their high output force, fast response, and small size. The vibration suppression of lightweight structures based on piezoelectric materials has been intensively studied, but vibration control for high-stiffness heavy structures is rare. In this work, a novel piezoelectric cantilever beam structure characterized by a large size, high mass and high stiffness was designed. It incorporates a new type bending moment piezoelectric stack actuator, which features an exceptionally high output bending moment, as well as reliability and maintainability in harsh environments. On the basis of the structure of the piezoelectric stack actuator, an equivalent mechanical model of the actuator was derived. The state-space equation of the piezoelectric cantilever beam was subsequently obtained, and a new linear quadratic regulator (LQR) was designed. On the basis of the controllability criterion and modal force maximization criterion, an optimized layout design of the piezoelectric cantilever beam was completed and experimentally validated on a large, heavy and stiff piezoelectric cantilever beam. This work provides a solid theoretical and experimental basis for the application of small-strain, high-stress piezoelectric materials in the vibration suppression of high-stiffness heavy cantilever structures.

ARTICLE HISTORY
Received 11 December 2024
Accepted 13 February 2025

KEYWORDS
Piezoelectric cantilever beam; active vibration control; piezoelectric stack actuator; optimized layout design; LQR

1. Introduction

In the fields of aerospace, civil and mechanical engineering, vibration suppression is an inevitable problem for most engineering structures especially with a high-precision control system [1–3]. Cantilever beam, the most widely used engineering structure, is trapped with forced and redundant vibration while working which is of heightened interest for both academia and industry. Most high-frequency vibrations of cantilever beams can be suppressed by passive vibration isolation. But it is unattainable for low frequency [4].

An increasing number of researchers are utilizing piezoelectric materials for the low frequency vibration suppression of cantilever structures because of their advantages of high output force, small size and fast response [5–8]. Tuma et al. modeled active vibration control for a thin mechanical structure as a cantilever beam with bonded piezoelectric patches. The transversal linear force produced by a linear piezo-actuator is replaced by the moment of force produced by the patch piezo-actuator, which is glued to the surface of the thin structure [9]. Raza et al. proposed a vibration suppression technique that used Macro Fiber Composite (MFC) to restrict the dynamic amplitudes of a cantilever beam [10]. Shen et al. conducted a study on vibration suppression of the blisk based on intentional mistuning of piezoelectric shunt damping patches [7]. Celia et al. developed a feedback algorithm that involved two piezoelectric actuators and two piezoelectric sensors for the control of the lowest four resonances of cantilever beam [11]. However, the vibration suppression is achieved by pasting or embedding a single piezoelectric sheet into the cantilever beam structure and the piezoelectric sheet can only be driven in the d_{13}/d_{31} mode rather than the d_{33} mode which has a higher piezoelectric coefficient [12–14]. It is hard to drive a beam structure that is much thicker than the piezoelectric sheet or has a certain rigidity. The design of the offset piezoelectric stack actuator offers several advantages over traditional piezoelectric wafers, which are listed and discussed in detail in Ref. [15], literature related to its cantilever applications is currently scarce, much less if considering experimental tests and validation. Among the very few examples, Song et al. developed a novel piezoelectric actuator operating in d_{33} mode for driving cantilever beams on high-end equipment [16]. Callipari et al. mounted a piezoelectric stack actuator on a cantilever plate representing a solar panel for experimental verification [17]. Zhou et al. implemented active vibration control of the cantilever sting based on piezoelectric stack actuators and velocity feedbacks using

CONTACT Xin Lan lanxin@hit.edu.cn Centre for Composite Materials and Structures, Harbin Institute of Technology, Harbin 150080, People's Republic of China; Yanju Liu yj_liu@hit.edu.cn Department of Astronautical Science and Mechanics, Harbin Institute of Technology, Harbin 150001, People's Republic of China.

accelerometers [18]. But, the main experimental object of vibration suppression is based on a thin cantilever beam structure, which cannot reflect the vibration characteristics of high-stiffness heavy cantilever structures in engineering applications, such as wind turbine blades, aircraft wings, and high-precision CNC machine cantilevers [19,20]. This discrepancy creates a significant gap between vibration suppression research and practical application [21–23]. Further research should be carried out on how to use the characteristics which are small strain and large stress of piezoelectric materials to suppress the vibration for high-stiffness heavy cantilever beam structures.

The better the actuator layout is, the better the control performance of a system [24–28]. Zhu et al. reviewed morphing structures driven by macro-fiber composites and analyzed their advantages and limitations. [29]. Bruant et al. formulated the optimal location and number of piezoelectric sensors for active vibration control using a genetic algorithm [30]. Lu et al. used the pole configuration method to study the optimized layout of actuators in large thin-plate structures [31]. Researchers have proposed many actuator optimization design methods based on various optimization criteria. However, different piezoelectric actuator layout optimization problems still exist for different smart piezoelectric structures [32]. A linear quadratic regulator is an effective control method for intelligent piezoelectric structures [33,34]. Chhabra et al. studied vibration suppression for a simply supported plate with piezoelectric patches at optimal positions to suppress the first specified modes using an LQR controller [35]. The core goal of linear quadratic optimal control is to minimize the objective function. A reasonable selection of the weighting coefficients Q and R will lead to better control system performance. Lu et al. explored the effects of different weighting factors, Q and R, on a system in their study of lightweight thin-film plate mirrors [36]. Afshar et al. designed the weighting coefficients Q and R to obtain an optimal feedback matrix in their study of electromagnetic levitation system [37]. However, in many application scenarios, there is no exact rule for selecting the weighting coefficients, and debugging is usually based on experience [38].

In summary, the vibration suppression of lightweight cantilever structures based on piezoelectric materials has been intensively studied, but vibration control for high-stiffness heavy structures is rare. The main previous experimental object of vibration suppression is based on a thin cantilever beam structure, which cannot reflect the vibration characteristics of high-stiffness heavy cantilever structures in engineering applications, such as wind turbine blades, aircraft wings, and high-precision CNC machine cantilevers. This discrepancy creates a significant gap between vibration suppression research and practical application. In addition, while there is considerable research on the optimal placement of surface-mounted piezoelectric sensors and actuators on smart beam structures, there is limited work on the layout optimization of BPSA. To address this research gap, this manuscript designed a new type of bending moment piezoelectric stack actuator for suppressing vibrations in high-stiffness, heavy cantilever structures. The state-space equations of a piezoelectric cantilever beam were obtained on the basis of an equivalent mechanical model of the piezoelectric stack actuator. The Q and R matrices were chosen to minimize the displacement at the end of the cantilever beam, and a new linear quadratic regulator (LQR) was obtained. On the basis of the controllability criterion and the criterion for maximizing modal force, an optimized layout design of the piezoelectric cantilever beam was completed and experimentally validated on a large-size, high-mass and high-stiffness piezoelectric cantilever beam. This work provides a solid theoretical and experimental basis for the application of small-strain, high-stress piezoelectric materials in vibration suppression of high-stiffness heavy cantilever structures.

2. Bending moment piezoelectric stack actuator

2.1. Design and modeling of a bending moment piezoelectric stack actuator

A bending moment actuator usually uses Macro Fiber Composite (MFC) to generate driving moments by attaching it to the surface of the structures to be controlled. However, the output bending moment of this actuator is very small, which is suitable only for small thin-walled structures and not for large-size, high-mass and high-stiffness engineering structures. Under the same input voltage, the output force of a piezoelectric stack is significantly greater than that of an MFC. However, converting the axial output force of the piezoelectric stack into a driving moment to suppress the bending vibrations of a beam is challenging. To address this problem, a new bending moment actuator based on a piezoelectric stack actuator is developed in this manuscript, which can convert the axial force of the piezoelectric stack actuator into driving moments acting on engineering structures. The novel Bending Moment Piezoelectric Stack Actuator (BPSA) has several advantages over the Macro Fiber Composite (MFC). The BPSA produces a significantly higher output bending moment than the MFC, allowing it to effectively control high-stiffness structures. Unlike the MFC, which is permanently adhered to a structure's surface and cannot be replaced, the BPSA enables easy coupling with other structures, simplifying maintenance and replacement of the piezoelectric stack. Additionally, its encapsulated piezoelectric ceramics ensure stable operation in challenging environments, including exposure to oil, water, and salt spray.

The BPSA consists of a piezo stack actuator, force transducer, preloader, left connector, and right connector. This assembly converts the axial force generated by the piezo stack actuator into a bending moment that acts on a cantilever beam. The piezo stack actuator consists of a piezo stack, a disk spring, a package housing, and an output side. The structural components and equivalent mechanical model of the piezo stack actuator are shown in Figure 1. The relevant parameters of the BPSA are shown in Table 1. The piezoelectric stack produces an inverse piezoelectric effect in response to the input voltage. The force of the piezo stack is divided into two parts, one part is transferred

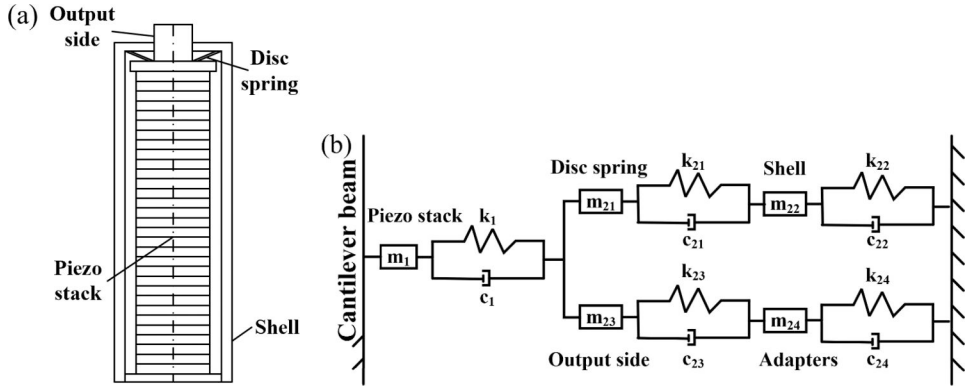

Figure 1. Modeling of piezoelectric stack actuator. (a) Design diagram. (b) Equivalent mechanical model diagram.

Table 1. BPSA parameters.

Parameter	Value
PZT diameter/mm	25
Maximum dynamic displacement/μm	60
Maximum output force/N	12000
Maximum operation voltage/V	1000
Maximum operating temperature/°C	200
Thickness of single ceramic layer/mm	0.5
Elastic compliance coefficient/(m^2/N)	18.5×10^{-12}
Piezoelectric charge coefficient/(C/N)	440×10^{-12}
Disk spring stiffness/(N/μm)	11.1
Shell stiffness/(N/μm)	489.94
Output side stiffness/(N/μm)	560
Adapters stiffness/(N/μm)	497.04

to the package housing through the disk spring and the other part is applied to the structure to be controlled through the output side. The output side is connected in series with the control object *via* adapters. The structural components and equivalent mechanical model of the BPSA are shown in Figure 2.

When the input voltage of the piezoelectric actuator is V and the preload force of the preloader is p, the deformation of the piezoelectric stack can be written as [39].

$$\delta_P = n(d_{33}V - hp/c_{33}^E A_P) \tag{1}$$

where n is the number of piezoelectric wafers, d_{33} is the piezoelectric strain constant, h is the thickness of a single wafer, c_{33}^E is the stiffness coefficient of the piezo stack, and A_P is the cross-sectional area of the piezo stack.

The internal strain of the piezoelectric stack can be expressed as

$$\varepsilon_P = \frac{\delta_P}{l_P} = \frac{n}{n \cdot h}\left(d_{33}V - hp/c_{33}^E A_P\right) = d_{33}V_P/h - p/c_{33}^E A_P \tag{2}$$

where l_P is the length of the piezo stack.

According to Hooke's law, the internal axial force of the stack can be obtained:

$$F_P = E_P \varepsilon_P A_P = E_P\left(d_{33}A_P V_P/h - p/c_{33}^E\right) \tag{3}$$

where E_P is the elastic modulus of the piezoelectric material.

The piezoelectric stack output force and displacement can be written as

$$F_{out} = F_P \times \frac{k_{23}k_{24}}{k_{23}+k_{24}} \Big/ \left(\frac{k_{21}k_{22}}{k_{21}+k_{22}} + \frac{k_{23}k_{24}}{k_{23}+k_{24}}\right) \tag{4}$$

$$u_{out} = \frac{F_{out}}{k_{23}} = E_P\left(d_{33}A_P V_P/k_{23}h - p/k_{23}c_{33}^E\right) \tag{5}$$

where k_{21} is the rigidity of the disk spring, k_{22} is the rigidity of the shell, k_{23} is the rigidity of the output side, and k_{24} is the rigidity of the adapters.

The bending moment generated by the BPSA can be written as

$$M_{BPSA} = F_{out} \bullet y = E_P y\left(d_{33}A_P V_P/h - p/c_{33}^E\right) \frac{k_{23}k_{24}}{k_{23}+k_{24}} \Big/ \left(\frac{k_{21}k_{22}}{k_{21}+k_{22}} + \frac{k_{23}k_{24}}{k_{23}+k_{24}}\right) \tag{6}$$

where y is the distance between the axis of the piezoelectric stack actuator and the neutral surface of the cantilever beam.

The proportional relationships among the actuating moment, the installing height of the BPSA, the precompression force and the driving voltage are expressed in Eq. (6).

2.2. Mechanical modeling of high-stiffness heavy piezoelectric cantilever beams

The BPSA converts the axial force of the piezoelectric stacked actuator into a driving bending moment to act on the cantilever beam and suppresses the vibration of the cantilever beam. The cantilever beam in this work is characterized by a large size, high mass and high stiffness (Figure 3). The length of the cantilever beam is 1200 mm, the width is 150 mm, and the thickness is 60 mm. The distances from the left end and the right end of the BPSA to the fixed end of the cantilever beam are x_1 and x_2, respectively. The specific parameters of the piezoelectric cantilever beam are shown in Table 2.

Modal analysis theory can convert physical coordinates into modal coordinates. When calculating the forced vibration response of a cantilever beam, modal analysis theory uses the orthogonality of the motion system eigenfunctions to substantially reduce the computational effort.

The transverse vibration of a cantilever beam under external loading is as follows

$$m\frac{\partial^2 w}{\partial t^2} + c\frac{\partial w}{\partial t} + ENTEEI\frac{\partial^4 w}{\partial x^4} = f(x,t) \tag{7}$$

The displacement of the structure is divided into a temporal component and a spatial component

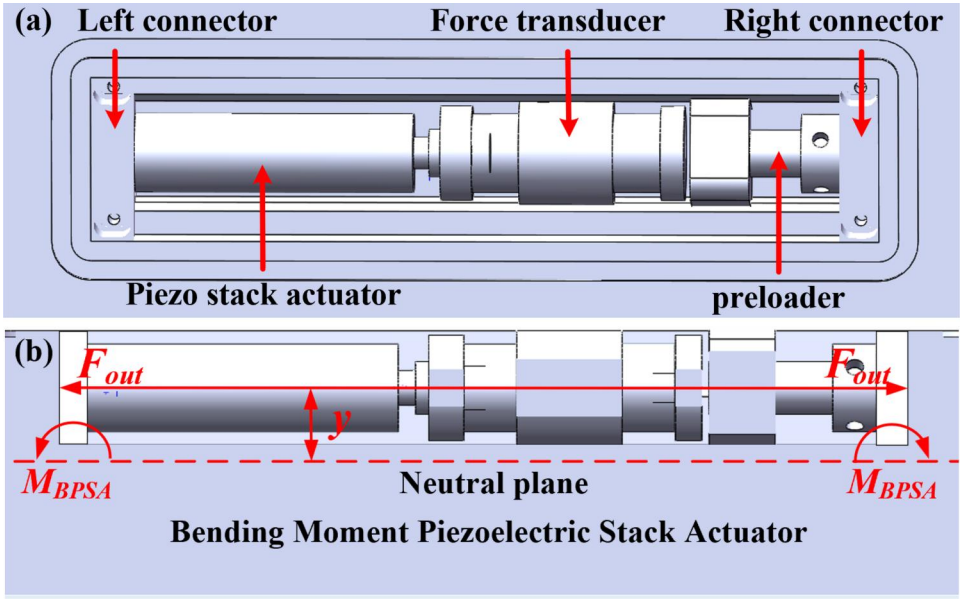

Figure 2. Modeling of the BPSA (a) design diagram. (b) Working principle diagram.

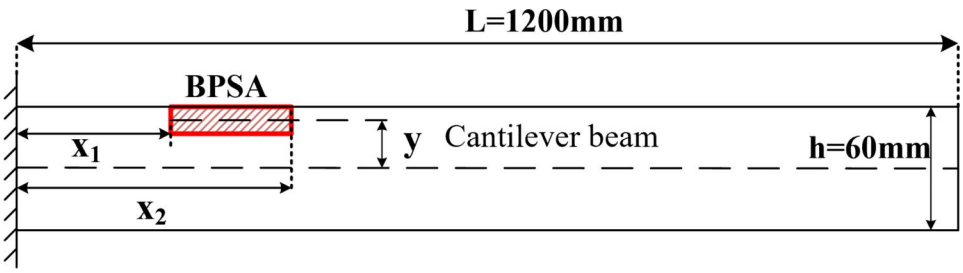

Figure 3. Modeling of piezoelectric cantilever beam.

Table 2. Piezoelectric cantilever beam parameters.

Parameters	Value
Length × width × height/(mm × mm × mm)	1200×150×60
density/(Kg/m^3)	7850
Elastic Modulus/GPa	206
Poisson's ratio	0.28

$$w(x,t) = \Phi(x)\eta(t) \tag{8}$$

The external force is expressed in the form of a vibration pattern as

$$f(x,t) = \sum_{i=1}^{\infty} f_i(t)\Phi_i(x) \tag{9}$$

By substituting Eq. (8) and Eq. (9) into Eq. (7),

$$\sum_{i=1}^{\infty}(m_i\Phi_i(x)\ddot{\eta}(t) + c_i\Phi_i(x)\dot{\eta}(t) + EI\Phi_i''''(x)\eta(t)) = \sum_{i=1}^{\infty} f_i(t)\Phi_i(x) \tag{10}$$

The equation for the transverse free vibration of a cantilever beam is as follows:

$$\begin{cases} EI\dfrac{\partial^4\Phi(x)}{\partial x^4} - m\omega^2\Phi(x) = 0 \\ \dfrac{\partial^2\eta(t)}{dt^2} + \omega^2\eta(t) = 0 \end{cases} \tag{11}$$

By substituting Eq. (11) into Eq. (10),

$$\sum_{i=1}^{\infty}(\Phi_i(x)\ddot{\eta}(t) + 2\zeta_i w_{ni}\Phi_i(x)\dot{\eta}(t) + {w_{ni}}^2\Phi_i(x)\eta(t)) = \sum_{i=1}^{\infty} f_i(t)\Phi_i(x)/m_i \tag{12}$$

Normalization vis vibrational orthogonality gives:

$$\int_0^L {\Phi_i}^2(x)dx = 1, i = 1,2,3\cdots \tag{13}$$

Equation (12) can be written as

$$\ddot{\eta}_i(t) + 2\zeta_i w_{ni}\dot{\eta}_i(t) + {w_{ni}}^2\eta(t) = f_i(t)/m_i \tag{14}$$

The disturbance and control forces applied to the cantilever are assumed to be $f_p(x,t)$ and $f_{con}(x,t)$.

$$f_p(x,t) = F_p(t)\ \ \delta(x - x_0) \tag{15}$$

$$f_{con}(x,t) = M_{con}(t)\frac{\partial}{\partial x}(\delta(x - x_2) - \delta(x - x_1)) \tag{16}$$

Therefore,

$$f(x,t) = f_p(x,t) + f_{con}(x,t) = F_p(t)\ \ \delta(x - x_0) + M_{con}(t)\frac{\partial}{\partial x}(\delta(x - x_2) - \delta(x - x_1)) \tag{17}$$

Multiplying both ends of Eq. (17) simultaneously by $\Phi_i(x)$, and integrating across the entire span of the beam results in a final value.

$$f_i(t)=\int_0^L f(x,t)\Phi_i(x)dx \tag{18}$$

By substituting Eq. (17) into Eq. (18),

$$\begin{aligned} f_i(t)=&\int_0^L F_p(t)\ \delta(x-x_0)\Phi_i(x)+M_{con}(t)\frac{\partial}{\partial x}(\delta(x-x_2)\\ &-\delta(x-x_1))\Phi_i(x)dx\\ =&F_p(t)\ \Phi_i(x_0)+M_{con}(t)(\Phi_i{}'(x_2)-\Phi_i{}'(x_1)) \end{aligned} \tag{19}$$

By substituting Eq. (19) into Eq. (14),

$$\begin{aligned} \ddot{\eta}_i(t)+2\zeta_i w_{ni}\dot{\eta}_i(t)+{w_{ni}}^2\eta(t)=&F(t)\Phi_i(x_0)/m_i\\ &+M_{con}(t)(\Phi_i{}'(x_2)-\Phi_i{}'(x_1))/m_i \end{aligned} \tag{20}$$

Assume that y is the distance from the driving force to the neutral plane of the cantilever.

$$M_{con}=M_{BPSA}=E_P y\left(d_{33}A_P V_P/h-p/c_{33}^E\right)\frac{k_{23}k_{24}}{k_{23}+k_{24}}\Big/\left(\frac{k_{21}k_{22}}{k_{21}+k_{22}}+\frac{k_{23}k_{24}}{k_{23}+k_{24}}\right) \tag{21}$$

The modal equations can be written as follows

$$\begin{bmatrix}\dot{\eta}(t)\\ \ddot{\eta}(t)\end{bmatrix}=\begin{bmatrix}0 & 1\\ -{w_i}^2 & -2\zeta_i w_i\end{bmatrix}\begin{bmatrix}\eta(t)\\ \dot{\eta}(t)\end{bmatrix}+\begin{bmatrix}0\\ \dfrac{(\Phi_i{}'(x_2)-\Phi_i{}'(x_1))}{m_i}\end{bmatrix}M_{BPSA}(t)+\begin{bmatrix}0\\ \dfrac{\Phi_i(x_0)}{m_i}\end{bmatrix}F(t) \tag{22}$$

2.3. Design of the active vibration controller

2.3.1. State-space equations of the piezoelectric cantilever beam

Introducing the state vector $x_i(t)=[\eta_i(t)\ \dot{\eta}_i(t)]^T$, the state-space equation is as follows:

$$\dot{x}(t)=Ax(t)+B_pF(t)+B_{con}M_{BPSA}(t) \tag{23}$$

where $A=\begin{bmatrix}0 & 1\\ -{w_i}^2 & -2\zeta_i w_i\end{bmatrix}$, $B_p=\begin{bmatrix}0\\ \dfrac{\Phi_i(x_0)}{m_i}\end{bmatrix}$, and $B_{con}=\begin{bmatrix}0\\ \dfrac{(\Phi_i{}'(x_2)-\Phi_i{}'(x_1))}{m_i}\end{bmatrix}$.

The deflection value of the free end is as follows

$$y(l_b,t)=\sum_{i=1}^{n}\Phi_i(l_b)\eta_i(t) \tag{24}$$

The end displacement is chosen as the output of the vibration system, then the state output variable is defined as

$$y(t)=Cx(t) \tag{25}$$

where $C=\begin{bmatrix}\Phi_i(l_b) & 0\end{bmatrix}$.

The state-space equation of the system is as follows:

$$\begin{cases}\dot{X}(t)=Ax(t)+B_{con}M_{BPSA}(t)+B_pF(t)\\ Y(t)=CX(t)\end{cases} \tag{26}$$

2.3.2. Design of the linear quadratic optimal regulator

The essential problem of the LQR is to determine the best control law that minimizes the performance function. In the performance function, the 1st integral term serves to minimize the error, and the 2nd integral term serves to minimize the energy input. The system will produce different optimal solutions for different choices of the Q and R weighting matrices. The performance of the control system is intricately linked to the choice of Q and R. The performance function of the LQR is as follows

$$J=\int_{t_0}^{t_1}\left[x^T(t)Qx(t)+u^T(t)Ru(t)\right]dt \tag{27}$$

where Q represents the matrix for weighting the state variable. R represents the matrix for weighting the input variables.

This method uses the terminal displacement of the cantilever as a measure of vibration severity. Therefore, a displacement sensor was chosen to capture the final deflection. The matrices for weighting the state variables and input variables are detailed below.

$$Q=C'*C \tag{28}$$

$$R=1\times e^{-12}*\mathrm{eye}(N_C) \tag{29}$$

where N_C is the number of linear quadratic optimal regulators.

Once the performance function is determined, the essence of resolving the optimal problem is to solve the extreme value of the performance function. The performance function is constrained by the equation of state of the system. The Hamilton matrix is established as follows

$$\begin{aligned} H=&\frac{1}{2}\left[x^T(t)Qx(t)+u^T(t)Ru(t)\right]\\ &+\lambda^T(t)(A(t)x(t)+B(t)u(t)) \end{aligned} \tag{30}$$

where $\lambda(t)$ is the Lagrange multiplier.

The state-space equation is as follows:

$$\dot{x}(t)=\frac{\partial H}{\partial\lambda}=A(t)x(t)+B(t)u(t) \tag{31}$$

The covariance equation is as follows:

$$\dot{\lambda}(t)=-\frac{\partial H}{\partial x}=-Q(t)x(t)-A^T(t)\lambda(t) \tag{32}$$

The necessary conditions for optimal control are as follows:

$$\frac{\partial H}{\partial u} = R(t)u(t) + B^T(t)\lambda(t) = 0 \tag{33}$$

The optimal control signal can be derived from Eq. (33). The optimal solution of the performance function is as follows:

$$u(t)^* = -R^{-1}(t)B^T(t)\lambda(t) \tag{34}$$

According to optimal control theory, the relationship between $\lambda(t)$ and $x(t)$ is as follows:

$$\lambda(t) = P(t)x(t) \tag{35}$$

$P(t)$ fulfills the Riccati differential equation:

$$\dot{P}(t) = -P(t)A(t) - A^T(t)P(t) + P(t)B(t)R^{-1}(t)B^T(t)P(t) - Q(t) \tag{36}$$

The optimal control signals are as follows:

$$u(t)^* = -R^{-1}(t)B^T(t)P(t)x(t) = -G_x(t)x(t) \tag{37}$$

where $G_x(t)$ is the feedback gain matrix.

In the steady-state case, the state of the system asymptotically converges to zero, and the solution of the Riccati differential equation asymptotically converges to a constant. After the system has stabilized, the Riccati differential equation is simplified as follows:

$$PA + A^TP - PBR^{-1}B^TP + Q = 0 \tag{38}$$

The LQR function can be used to solve the optimal control in the numerical simulation software. The LQR function is implemented as follows:

$$\text{Syntax} : [G_x, P, e] = lqr(A, B, Q, R) \tag{39}$$

where e is the eigenvalue of the closed-loop system.

3. Optimized layout design of the piezoelectric cantilever beam

A reasonable placement of an actuator in a controlled structure can achieve excellent control effects with less power consumption. The cost of a single BPSA is relatively low, and its weight is only about 350 g, which does not impact the overall structure's weight. The BPSA enables easy coupling with the controlled structures, simplifying maintenance and replacement of the piezoelectric stack, making it easy to implement. Therefore, this section studies the layout optimization of piezoelectric stack actuators on the base of the controllability criterion and modal force maximization criterion.

3.1. Optimized layout design based on controllability criteria

The concept of controllability was first introduced by Kalman. It plays an important role in modern control theory. In this section, an optimized layout design of actuators was studied according to the controllability index. This index measures the control capability of the actuator under a given input voltage.

From the state-space equations of the system, the control forces acting on the system are as follows:

$$\{f\} = [B]\{u\} \tag{40}$$

The magnitude of the control force can be expressed as

$$\{f\}^T\{f\} = \{u\}^T[B]^T[B]\{u\} \tag{41}$$

The singular value decomposition of matrix B is

$$B = MSN^T \tag{42}$$

where $MM^T = M^TM = E, NN^T = N^TN = E, S = \begin{bmatrix} \sigma_1 & 0 & 0 & 0 \\ 0 & \sigma_2 & 0 & 0 \\ 0 & 0 & \ddots & 0 \\ 0 & 0 & 0 & \sigma_k \end{bmatrix}$

By substituting Eq. (41) into Eq. (40):

$$\{f\}^T\{f\} = \{u\}^TNS^2N^T\{u\} \tag{43}$$

where $S^2 = \begin{bmatrix} {\sigma_1}^2 & 0 & 0 & 0 \\ 0 & {\sigma_2}^2 & 0 & 0 \\ 0 & 0 & \ddots & 0 \\ 0 & 0 & 0 & {\sigma_k}^2 \end{bmatrix}$

Introducing an emerging input vector gives

$$v = N^T\{u\} \tag{44}$$

The input vector is equivalent to the original control input vector $\{u\}$ in terms of energy. Equation (42) can be represented as

$$\{f\}^T\{f\} = v^TS^2v = \sum_{i=1}^{k} {\sigma_i}^2{v_i}^2 \tag{45}$$

where σ_i is the singular value of the input matrix.

σ_i varies with the location of the actuator. Introducing the controllability index gives

$$\Omega_i = |\sigma_i| \tag{46}$$

Therefore, the larger the controllability index is, the greater the control force of the driver on the cantilever beam. The controllability index of the model is solved to determine the optimal control location of the actuator. The control input matrix of this manuscript is as follows:

$$B_{con} = \begin{bmatrix} 0 \\ \dfrac{(\Phi_i'(x_2) - \Phi_i'(x_1))}{m_i} \end{bmatrix} \tag{47}$$

Singular value decomposition is performed on the control input matrix to obtain the singular values as follows:

$$\sigma_i = \frac{1}{m_i}(\Phi_i'(x_2) - \Phi_i'(x_1)) \tag{48}$$

When the actuator is significantly shorter than the cantilever beam, Eq. (47) can be expressed as

$$\sigma_i = \frac{\Delta x}{m_i}(\Phi_i''(x_1)) \tag{49}$$

where Δx is the length of the actuator.

The controllability index can be expressed as

$$\Omega_i = \left| \frac{\Delta x}{m_i} (\Phi_i''(x_1)) \right| \tag{50}$$

The variation law of the controllability index is the same as that of $\Phi_i''(x_1)$ from Eq. (48). Therefore, the larger the absolute value of $\Phi_i''(x_1)$ is, the larger the controllability index, and the better the controllability of the system. The optimal control position of the actuator is determined according to the controllability index.

3.2. Optimized layout design based on the modal force maximization criterion

The principle of vibration suppression *via* actuators involves the actuator outputting a force in the opposite direction of the structure's vibration, thus counteracting the deformation and vibration of the structure. Therefore, we should place the actuator where the deformation of the system is the largest. The principle of the modal force maximization criterion is to place the actuator at the highest modal deformation of the beam, thus generating the maximum modal control force of the structure and obtaining the best control [40].

According to cantilever beam mode theory, the deflection response of a cantilever beam from the application of a unit moment excitation is presented below:

$$w(x, x_i) = \sum_{i=1}^{N} \frac{\Phi_i(x)\Phi_i'(x_i)}{m_i \Omega_i^2 (1 - \overline{w_i}^2 + 2j\xi_i \overline{w_i})} \tag{51}$$

where m_i represents the ith order modal mass; Ω_i represents the ith order natural frequency; ξ_i represents the ith order damping ratio; $\Phi_i(x)$ represents the ith order intrinsic vibration; and $\overline{w_i} = k/\Omega_i$.

Under the action of the BPSA, the displacement at the free end of the cantilever beam is as follows:

$$w(x, x_1, x_2) = M_{BPSA} \sum_{i=1}^{N} \frac{\Phi_i(x)(\Phi_i'(x_2) - \Phi_i'(x_1))}{m_i \Omega_i^2 (1 - \overline{w_i}^2 + 2j\xi_i \overline{w_i})} \tag{52}$$

When the actuator is significantly shorter than the beam's length, Eq. (57) can be expressed as

$$w(x, x_1, x_2) = M_{BPSA} \Delta x \sum_{i=1}^{N} \frac{\Phi_i(x)\Phi_i''(x_1)}{m_i \Omega_i^2 (1 - \overline{w_i}^2 + 2j\xi_i \overline{w_i})} \tag{53}$$

Therefore, when the absolute value of $\Phi_i''(x_1)$ is taken as the maximum value, the maximum modal response for the ith order modal generalized force excitation can be obtained. The BPSA can induce the maximum ith order modal response.

According to material mechanics, the strain is related to the deflection as follows

$$\begin{aligned} \varepsilon = \frac{y}{\rho} &= y \frac{\partial^2 w(x, x_1, x_2)}{\partial x^2} \\ &= M_{BPSA} y \Delta x \sum_{i=1}^{N} \frac{\Phi_i''(x)\Phi_i''(x_1)}{m_i \Omega_i^2 (1 - \overline{w_i}^2 + 2j\varepsilon_i \overline{w_i})} \end{aligned} \tag{54}$$

Equation (52) shows that the strain in the cantilever beam is greatest when the absolute value of $\Phi_i''(x_1)$ is greatest, which means that the BPSA should be placed there.

The inherent frequency equation of the cantilever beam is as follows:

$$\cos(k_i L_x) g \cosh(k_i L_x) + 1 = 0 \tag{55}$$

The vibration function equation for the cantilever beam is as follows:

$$\Phi_i(x) = \cosh(k_i x) - \cos(k_i x) - \beta_n (\sinh(k_i x) - \sin(k_i x)) \tag{56}$$

where $\beta_n = \frac{\cosh(k_i L_x) - \cos(k_i L_x)}{\sinh(k_i L_x) - \sin(k_i L_x)}$.

The graph of $\Phi_i''(x)$ $(i = 1, 2, 3)$ is plotted in Figure 4.

Consistent conclusions were derived on the base of controllability criterion and the modal force maximization criterion. For the first-order modes, the optimal control location is at the root of the cantilever beam. For the second-order mode, the optimal control location remains at the root of the cantilever beam, with a secondary control location at $x = 0.53$L. For the third-order mode, the optimal control location is at the root of the cantilever beam, with secondary and tertiary control locations at $x = 0.71$L and $x = 0.31$L respectively.

4. AVC simulation of piezoelectric cantilever beam

Researchers have conducted numerous studies on the vibration suppression of cantilever beams and reported that the majority of the energy is concentrated in the first-order mode when a cantilever beam undergoes low-frequency vibration [2]. The piezoelectric cantilever beam in this study (1200 mm in length, 150 mm in width, and 60 mm in thickness) has a large size and mass, which makes it more prone to low-frequency vibration. In this section, the first-order mode vibration is taken as the target for vibration suppression. The effects of different numbers of BPSAs and

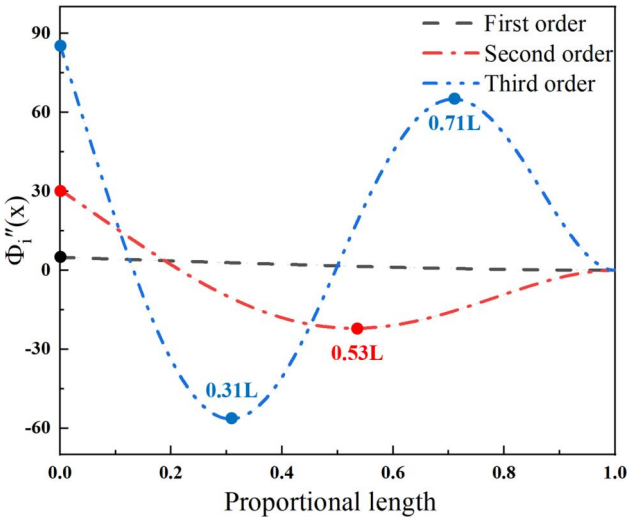

Figure 4. Second-order derivative curve of the oscillatory function with respect to x.

different placement positions on the suppression of first-order mode vibrations were studied. An attempt was also made to simultaneously suppress the first three orders of modal vibration of the cantilever beam *via* a single actuator. The layout optimization design was simulated and validated *via* linear quadratic regulators.

4.1. Optimized layout design simulation verification of a single piezoelectric actuator

The LQR is well suited for controlling the first few orders of the system modalities. In this section, a single BPSA was simulated with a linear quadratic regulator. The BPSA was placed at different control positions to study the effect of the control position on the vibration characteristics of the system. The active control effect was reflected by the vibration suppression rate of the cantilever beam. The LQR controller was placed at 0.1, 0.2, 0.3, 0.31, 0.4, 0.5, 0.53, 0.6, 0.7, 0.71, 0.8, 0.9, or 1.0 L. The optimized design of a single BPSA layout was verified. The simulation results are displayed in Figure 5.

The numerical simulation revealed the vibration suppression effect of the cantilever beam when the LQR was 0.1, 0.2, 0.3, 0.31, 0.4, 0.5, 0.53, 0.6, 0.7, 0.71, 0.8, 0.9, or 1.0 L, as shown in Table 3.

The simulation of the layout optimization for a single actuator indicates that the optimal control effect is achieved when the actuator is positioned at the root, resulting in a vibration suppression rate of 97.07%. As the actuator is moved further from the root, the control effectiveness progressively diminishes, with a rapid decline in control performance observed when the actuator is positioned beyond the midpoint.

4.2. Optimized layout design simulation verification of multiple piezoelectric actuators

To investigate the effect of two BPSAs at different arrangement positions on the vibration control of a cantilever beam, we refer to the optimized layout design from the previous analysis. For the first-order modes, the optimal control location is at the root of the cantilever beam. For the second-order mode, the optimal control location remains at the root of the cantilever beam, with a secondary control location at $x = 0.53$L. For the third-order mode, the optimal control location is at the root of the cantilever beam, with secondary and tertiary control locations at $x = 0.71$L and $x = 0.31$L respectively. In high-stiffness heavy cantilever structures, the fixed end is typically the power side, such as in ship propellers and wind turbine blades, while the free end often serves as the operational side, such as in CNC machine tools, where installing controllers is inappropriate. Based on these considerations, LQR controllers were placed at 0.31 and 0.53 L, 0.31 and 0.71 L, and 0.53 and 0.71 L. The shaker position remained unchanged. The simulation results are displayed in Figure 6.

The numerical simulation revealed the vibration control effect when the linear quadratic regulators were located at 0.31 and 0.53 L, 0.31 and 0.71 L, and 0.53 and 0.71 L, as shown in Table 4.

A linear quadratic regulator was used to control the first three orders of modalities of the cantilever beam simultaneously. The shaker and linear quadratic regulator were

Table 3. Vibration suppression effects of cantilever beams based on a single piezoelectric actuator.

Layout location	Uncontrolled amplitude (μm)	Controlled amplitude (μm)	Vibration suppression rate
0.1L	36.92	1.08	97.07%
0.2L	36.92	1.35	96.34%
0.3L	36.92	1.73	95.31%
0.31L	36.92	1.78	95.18%
0.4L	36.92	2.29	93.80%
0.5L	36.92	3.17	91.41%
0.53L	36.92	3.52	90.47%
0.6L	36.92	4.60	87.54%
0.7L	36.92	7.10	80.77%
0.71L	36.92	7.45	79.82%
0.8L	36.92	11.79	68.07%
0.9L	36.92	20.57	44.28%
1.0L	36.92	31.93	13.52%

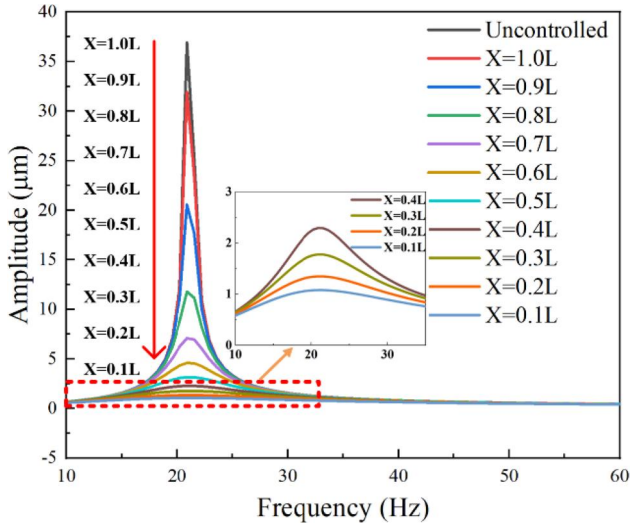

Figure 5. Amplitude response of the cantilever beam with the controller in different positions.

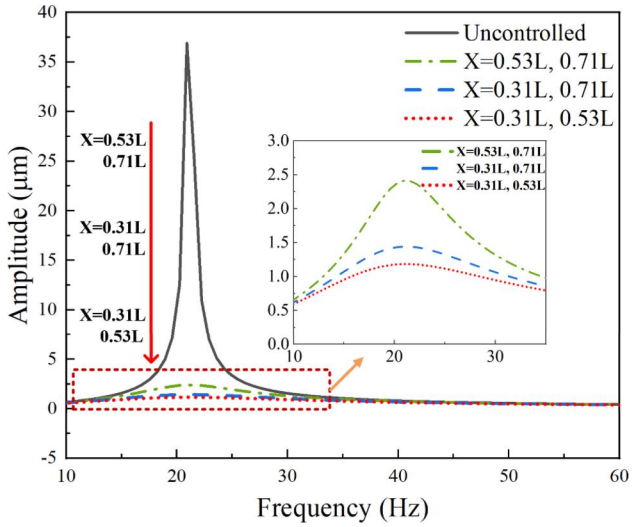

Figure 6. Amplitude response of the cantilever beam with the controllers in different positions.

Table 4. Vibration suppression effects of cantilever beams based on multiple piezoelectric actuators.

Layout location	Uncontrolled amplitude (μm)	Controlled amplitude (μm)	Vibration suppression rate
0.31,0.53L	36.92	1.18	96.80%
0.31,0.71L	36.92	1.44	96.10%
0.53,0.71L	36.92	2.41	93.47%

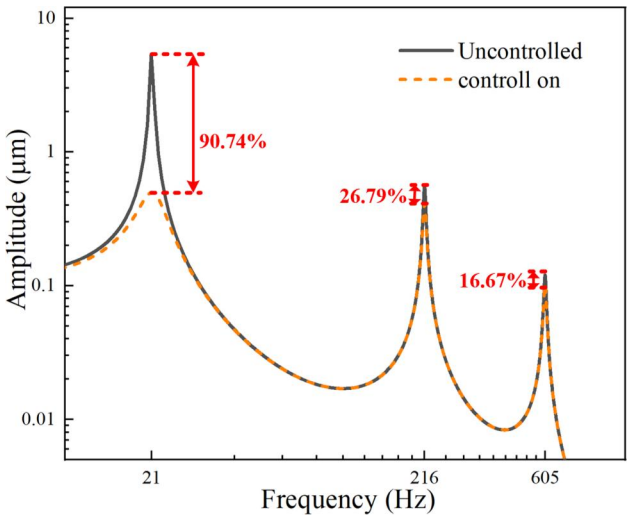

Figure 7. Vibration suppression effect of the first three order modes of the cantilever beam.

Table 5. Vibration suppression effect of the first three order modes of the cantilever beam based on a piezoelectric actuator.

Modal	Uncontrolled amplitude (μm)	Controlled amplitude (μm)	Vibration suppression rate
First order	5.40	0.50	90.74%
Second order	0.56	0.41	26.79%
Third order	0.12	0.10	16.67%

arranged at 0.31 L of the beam. The illustration in Figure 7 depicts the vibration suppression effect.

The simulation results when a linear quadratic regulator is used to control the first three orders of modalities of the cantilever beam simultaneously are shown in Table 5.

The simulation of the layout optimization design of multiple piezoelectric stack actuators leads to the conclusion that the vibration suppression rate exceeds 90% when two piezoelectric stack actuators are operating. Despite changing the arrangement position of the two piezoelectric actuators, the control effect is stable. The control effect gradually decreases as the control position moves away from the root. The suppression effect is obvious when the first three orders of the cantilever beam modalities are controlled simultaneously by a single actuator.

5. AVC experiment of piezoelectric cantilever beam

5.1. Piezoelectric stack actuator force-electric coupling performance test experiment

The piezoelectric stack actuator force-electric coupling performance test platform is made of steel. The high rigidity of the platform creates good measurement conditions for

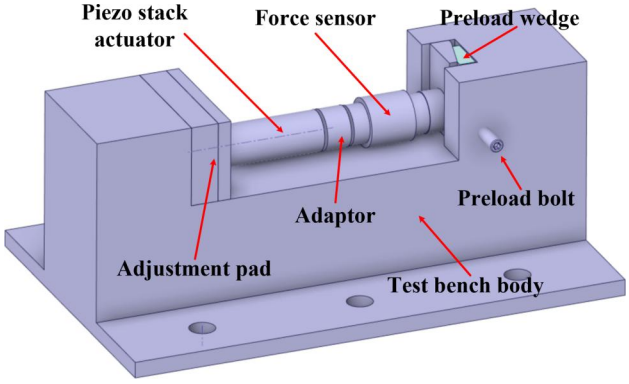

Figure 8. Piezoelectric stack actuator force-electric coupling performance test bench.

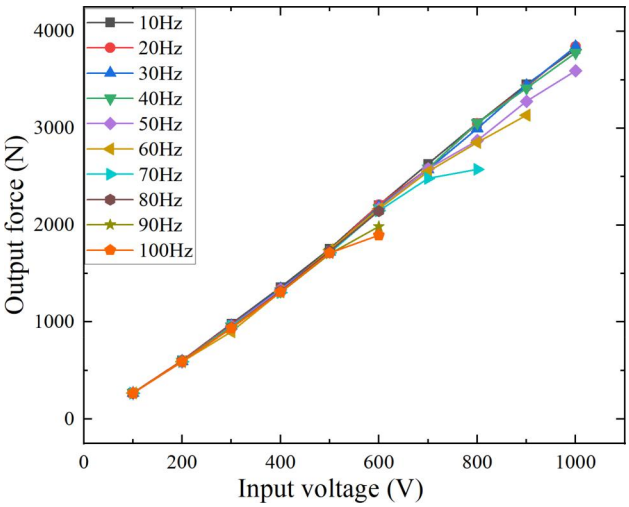

Figure 9. Output force of the piezoelectric stack actuator at different input voltages.

force-electric coupling performance testing of the actuator. The structure of the test bench is shown in Figure 8. The actuator's tail end is fastened to an adjustment pad. The actuator's output is linked to a pressure sensor (model CL-YD-2311) through an adapter. The large displacement adjustment is performed by the adjustment pad. A small displacement adjustment is carried out by pushing the preload wedge with the preload bolt. Pressure sensors capture the actuator's output force at different input voltages and input frequencies.

A piezoelectric stack actuator (diameter of 25 mm, length of 71 mm) was tested. The output force was tested at different input voltages and input frequencies, as shown in Figures 9 and 10.

The experimental results show that the output force increases linearly as the input voltage (less than or equal to 500 V) increases when the input frequency is taken as a fixed value. However, as the input voltage (greater than 500 V) increases, the linearity becomes worse. The output force remains stable as the input frequency increases when the input voltage is taken as a fixed value. However, when the input voltage is fixed (greater than 500 V), the output force decreases slightly increasing input frequency. One of the major reasons for the above phenomenon is that the output power of the power supply is insufficient as the input

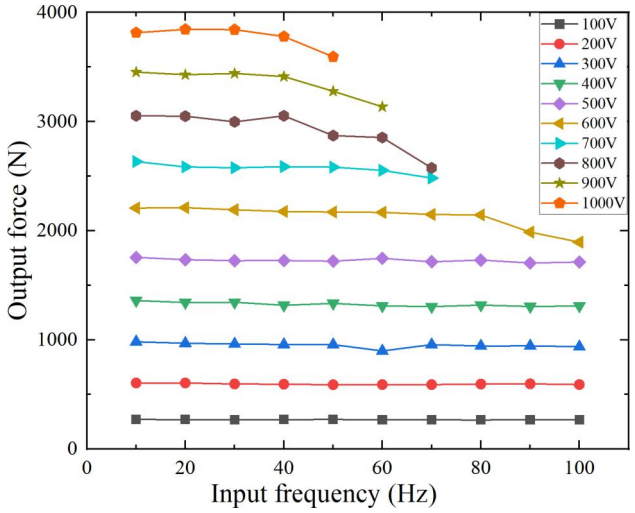

Figure 10. Output force of the piezoelectric stack actuator at different input frequencies.

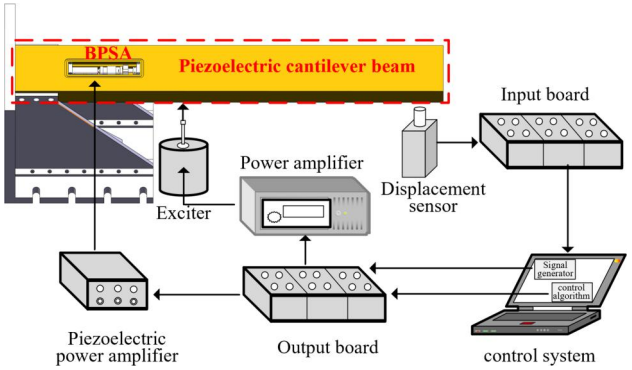

Figure 11. Experimental platform for active vibration control of the piezoelectric cantilever beam.

voltage and input frequency of the piezoelectric stack actuator increase.

5.2. Active vibration control experiment of high-stiffness heavy cantilever beams based on the BPSA

Since the cantilever beam is made of steel with a large size, high mass and high stiffness, it is imperative to design a fastening device with adequate rigidity and stability. The fixture consists of a right-angled steel plate and two trapezoidal ribs. The root of the piezoelectric cantilever beam is bolted to this device. The fixing device is attached to the cast iron platform by bolts. The shaker is connected to the cast iron platform by a fixed support. The structure of the active vibration suppression experimental platform is shown in Figure 11.

In this experiment, the shaker (model JZK-50) serves as the excitation source for the system. The displacement sensor (model ZA-21) takes the vibration displacement signal from the tail end of the beam and inputs it to the vibration signal processing system. The vibration signal processing system was outfitted with an 8-channel verified time controller (model PXIe-8881, equipped with a Linux RT real-time operating system), a 2-channel 24-bit analogue output dynamic signal generator (model PXIe-4463), and a 16-channel 24-bit dynamic signal acquisition card (model PXIe-4497). The vibration control system generates an optimal feedback signal to the actuator. The actuator generates an antiphase vibration to suppress the vibration of the piezoelectric cantilever beam. To ensure the reproducibility of the experiment, we conducted the tests during quiet periods with stable temperature and humidity conditions, which had almost no impact on the results. The primary source of measurement uncertainties in our study stems from reading errors, which were minimized by averaging multiple sets of data to reduce variability, and confidence intervals have also been added.

5.2.1. Modal test experiment with the piezoelectric cantilever beam

In this section, the hammering method was selected for the modal testing of the system. A force hammer was used to strike the hammering point, and the displacement sensor collected the displacement signal. A Fourier transform was performed in the data analyzer to obtain the intrinsic frequency of the system. The experimental results of the cantilever beam modal test are shown in Figure 12.

Modal testing of the cantilever beam was carried out *via* the hammering method. The displacement time domain information was subjected to fast Fourier variation to obtain the intrinsic frequency of the cantilever beam. The first-order inherent frequency of the system is 21 Hz.

5.2.2. Experiments on low-frequency active vibration control of high-stiffness heavy cantilever beams

An exciter is used as the excitation of the system, and a BPSA is used for vibration suppression of the cantilever beam. Displacement transducers are used to acquire the vibration signals. A data analyzer is used to analyze the vibration signals. The experimental system for active vibration control of the piezoelectric cantilever beam is shown in Figure 13.

In this experiment, the BPSA was positioned at the root of the beam. The vibration suppression effects at different vibration frequencies (5–50 Hz) are shown in Table 6. Additionally, the active vibration control effects of traditional PID control and LQR control at 10 Hz (noninvasive frequency) and 21 Hz (intrinsic frequency) were compared. The PID controller parameters K_p, K_i, K_d, and N were set to 0.5203, 4.0918, 0.0069, and 1000, respectively. The LQR control demonstrated improvements of 48.79% and 23.80%, respectively, compared to PID control at 10 Hz and 21 Hz, as shown in Figure 14.

The experimental results show that the vibration suppression rate is 72.47% when the vibration frequency is 21 Hz (intrinsic frequency). At different vibration frequencies, the vibration suppression rate of high-stiffness heavy piezoelectric cantilever beams is above 50%. The effect of active vibration control at low frequencies for high-stiffness heavy piezoelectric cantilever beams is obvious.

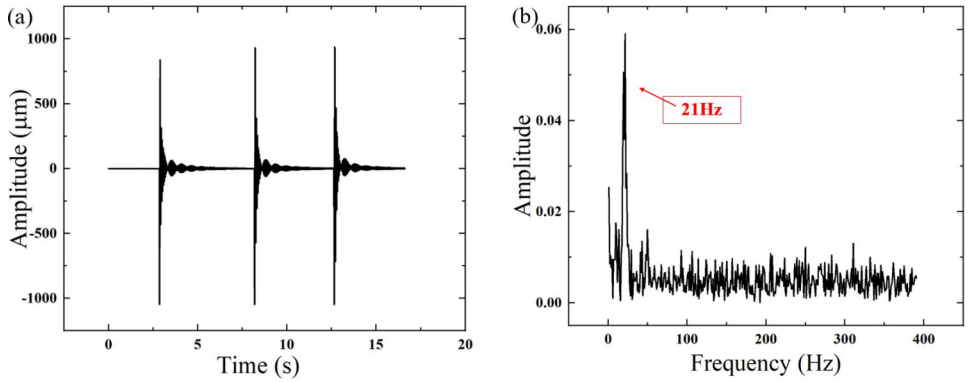

Figure 12. Modal experiment. (a) Time domain response. (b) Frequency domain response.

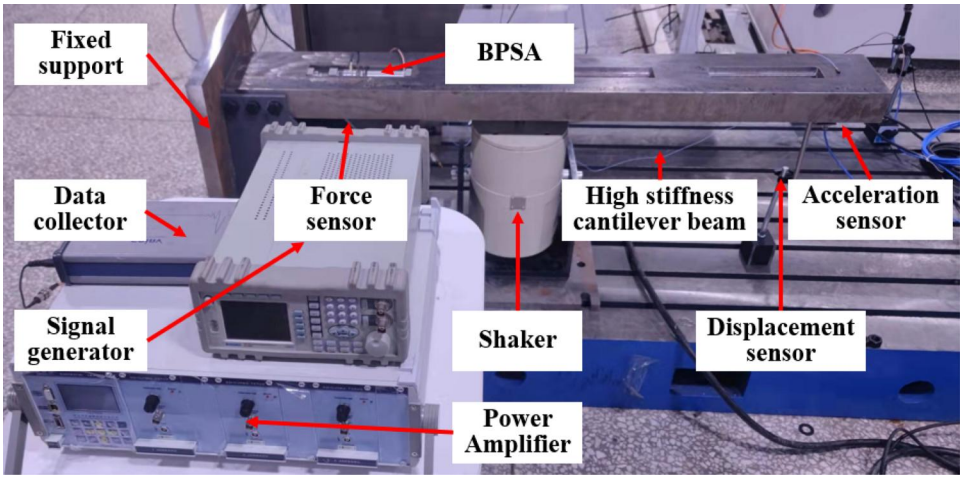

Figure 13. Active vibration control system of piezoelectric cantilever beam.

Table 6. Vibration suppression effects of different excitation frequencies.

Frequency (Hz)	Uncontrolled amplitude (μm)	Controlled amplitude (μm)	Vibration suppression rate
5	15.85	6.06	61.77%
10	18.98	6.52	65.65%
15	30.68	10.52	65.71%
21	30.77	8.47	72.47%
25	26.62	10.85	59.24%
30	11.22	4.12	63.28%
35	8.33	3.58	57.02%
40	5.64	2.42	57.09%
45	7.77	3.66	52.90%
50	7.71	3.74	51.49%

5.2.3. Experiments on the layout optimization design of a single piezoelectric actuator

The BPSA was arranged at different positions of the cantilever beam to verify the optimized layout of a single BPSA. The input frequency of the exciter and the BPSA was 21 Hz (intrinsic frequency). The vibration suppression effects at different positions of the cantilever beam are shown in Table 7. The BPSA was positioned at the root, middle or tail. The experimental results are shown in Figure 15.

The experimental results indicate that the vibration suppression rates are 72.47%, 62.45% and 56.01% when the BPSA is arranged at the root, middle and tail of the beam, respectively. As the BPSA is moved away from the fixed end of the cantilever beam, the control capability gradually decreases. Huang et al. conducted similar experiments, finding that under the same control parameters, the piezoelectric sheets require control voltages of 63 V and 75 V at 0.44 and 0.69 L, respectively, with the required voltage increasing as the distance from the fixed end increases, and that the control effect is worst at the free end, improving as the fixed end is approached, with smaller vibration amplitudes and better control [2]. The experiments effectively verify the optimized layout design of the single piezoelectric actuator.

From the energy point of view, the mechanical energy of the cantilever beam consists of kinetic energy and elastic potential energy. If we ignore the effect of damping, these two energies are converted to each other and their sum remains constant. If we can offset the elastic potential energy or kinetic energy of the cantilever beam system by inputting energy to the cantilever beam system through a piezoelectric stack actuator, then active vibration suppression of the cantilever beam system can be achieved. For a cantilever beam, its elastic potential energy is proportional to the square of the strain, and the maximum strain is generated at the point of maximum elastic potential energy. Therefore, arranging the piezoelectric stack actuator at the maximum strain of the cantilever beam can offset the elastic potential energy of the cantilever beam system to the maximum extent, and the active vibration control effect of the cantilever beam is the best. The maximum strain of a cantilever beam is located at the root, and the strain decreases as

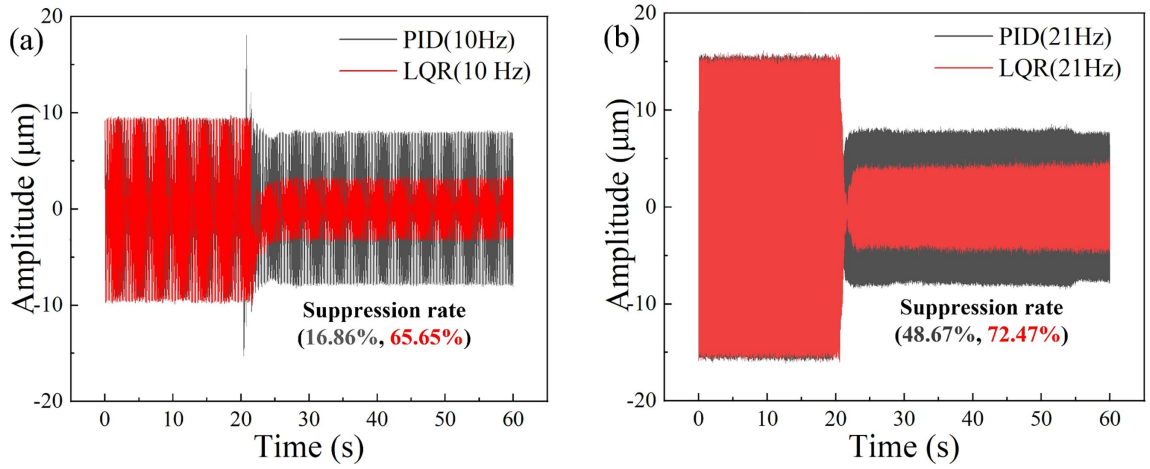

Figure 14. Vibration suppression effects of different excitation frequencies. (a) Noninvasive frequency. (b) Intrinsic frequency.

Table 7. Vibration suppression effects of different control positions.

Layout location	Uncontrolled average (μm)	Controlled amplitude (μm)	Controlled average (μm)	Confidence interval (95%)	Vibration suppression rate
Root	30.77	8.39	8.47	[8.30, 8.64]	72.47%
		8.50			
		8.52			
Middle	31.08	11.78	11.67	[11.43, 11.91]	62.45%
		11.59			
		11.64			
Tail	31.19	13.66	13.72	[13.54, 13.90]	56.01%
		13.70			
		13.80			

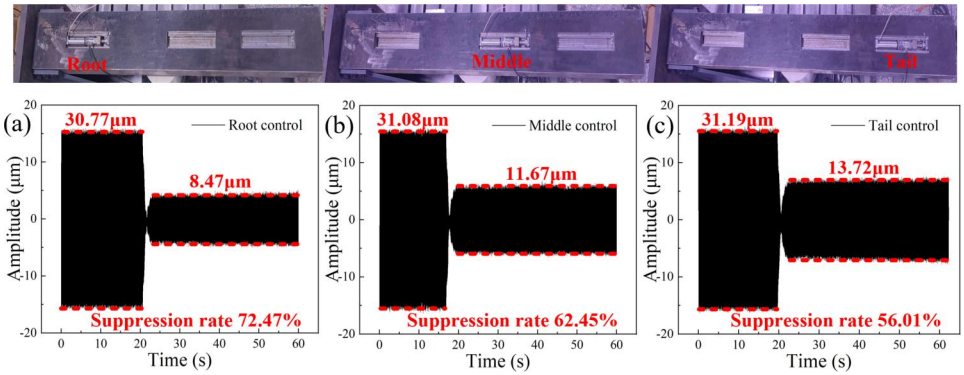

Figure 15. Vibration suppression effects of different control positions. (a) Root. (b) Middle. (c) Tail.

the distance from the root increases, leading to poorer control performance.

5.2.4. Experiments on optimized layout design of multiple piezoelectric actuators

The BPSAs were placed at the root and middle, root and tail, and middle or tail of the cantilever beam. These results were used to verify the optimized layout design of multiple piezoelectric actuators. The input frequency of the exciter and the BPSAs was 21 Hz (intrinsic frequency). The BPSAs were positioned at the root and middle, root and tail, and middle and tail of the piezoelectric cantilever beam. The vibration suppression effects at different positions of the cantilever beam are shown in Table 8. The experimental results are shown in Figure 16.

The experimental results indicate that the vibration suppression rates are 80.99%, 74.67% and 65.91% when the BPSAs are positioned at the root and middle, root and tail, middle and tail of the beam, respectively. As the BPSAs are moved away from the fixed end of the cantilever beam, the control capability gradually decreases. The experiment effectively verifies the optimized layout design of the multiple piezoelectric actuators.

5.2.5. Error analysis between simulation and experimental results

The AVC simulation results and the experimental results of the piezoelectric cantilever beam show some discrepancies. The vibration suppression rate in the simulation is 15.81%

Table 8. Vibration suppression effects of different control positions.

Layout location	Uncontrolled average (μm)	Controlled amplitude (μm)	Controlled average (μm)	Confidence interval (95%)	Vibration suppression rate
Root and middle	31.41	5.91	5.97	[5.79, 6.15]	80.99%
		5.95			
		6.05			
Root and tail	31.66	7.98	8.02	[7.80, 8.24]	74.67%
		7.96			
		8.12			
Middle and tail	31.77	10.77	10.83	[10.70, 10.96]	65.91%
		10.85			
		10.87			

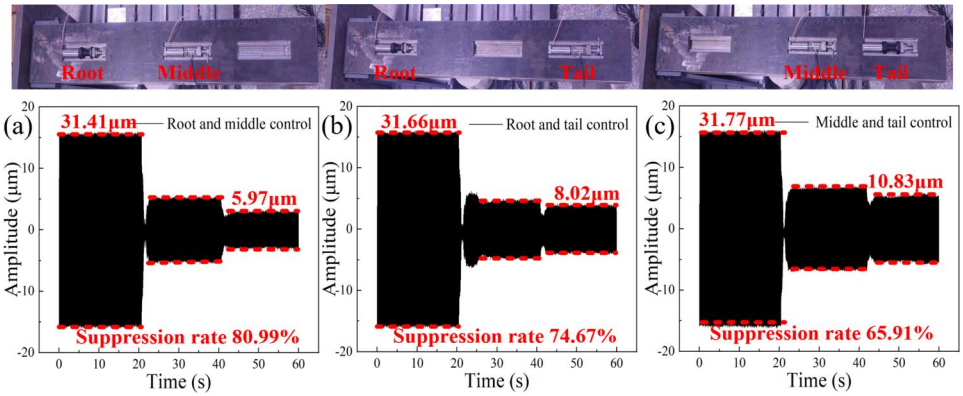

Figure 16. Vibration suppression effects of different control positions. (a) Root and Middle. (b) Root and tail. (c) Middle and tail.

Table 9. Error analysis between simulation and experimental results.

Layout location	Simulation suppression rate	Experimental suppression rate	Error
Root	95.18%	72.47%	22.71%
Middle	90.47%	62.45%	28.02%
Tail	79.82%	56.01%	23.81%
Root and middle	96.80%	80.99%	15.81%
Root and tail	96.10%	74.67%	21.43%
Middle and tail	93.47%	65.91%	27.56%

to 28.02% higher than in the experiment, as shown in Table 9.

The discrepancies between the simulation and experimental results can be attributed to several factors. First, the numerical model cannot fully capture the material properties of the piezoelectric material and its dynamic output characteristics, leading to deviations. Additionally, the simulation does not accurately represent experimental constraints such as contact stiffness, friction, and preload conditions, all of which influence the system's dynamic behavior. Moreover, the experiment is affected by factors such as the accuracy of the testing equipment and data transmission delays, whereas the numerical simulation operates under ideal control conditions. As a result, the suppression effect observed in the numerical simulation is higher than that in the experiment.

To improve the accuracy of numerical simulations, several aspects can be optimized. Incorporating experimentally obtained piezoelectric material properties and dynamic output characteristics into the numerical model is essential. Additionally, implementing more realistic experimental constraints, such as contact stiffness, friction, and preload conditions, should be considered in the simulation. System identification techniques can be employed to refine numerical parameters, thereby ensuring the simulation results align more closely with experimental observations. Furthermore, the use of high-resolution sensors and advanced data acquisition systems can enhance experimental accuracy, ultimately improving the effectiveness of active vibration control.

6. Conclusion

In this work, a bending moment piezoelectric stack actuator (BPSA) was designed, which greatly facilitates the coupling of the piezoelectric stack actuator and the structures as well as the maintenance and replacement of the piezoelectric stack without changing the shape of the original structure. On the basis of the encapsulated piezoelectric stack actuator structure, an equivalent mechanical model of the encapsulated piezoelectric stack was derived. The state–space equation of the piezoelectric cantilever beam was subsequently obtained. With the objective of minimizing the end displacement of the piezoelectric cantilever beam, the coefficient matrices Q and R were selected, and a linear quadratic regulator (LQR) was designed. The optimal control law for the first three orders of the piezoelectric cantilever beam modalities was obtained according to the controllability criterion and the modal force maximization criterion. Numerical simulations of the layout optimized design of single and multiple BPSAs show that as the BPSA is moved further from the root of the piezoelectric cantilever beam, the control effectiveness progressively diminishes. The experimental results show that low-frequency active vibration suppression effects of high-stiffness heavy piezoelectric cantilever beam

based on BPSAs is obvious. At different stimulation frequencies, the vibration suppression rate of the piezoelectric cantilever beam is above 50%. The vibration dampening rate is 72.47% when the vibration frequency is 21 Hz (inherent frequency). The experimental results of the optimized layout design show that the vibration suppression rates are 72.47%, 62.45% and 56.01% when the BPSA is arranged at the root, middle and tail of the cantilever beam, respectively. The vibration suppression rates are 80.99%, 74.67% and 65.91% when the BPSAs are positioned at the root and middle, root and tail, and middle and tail of the cantilever beam, respectively. The vibration suppression performance tends to decrease as the control position of the BPSAs moves away from the fixed end of the cantilever beam. This work provides a solid theoretical and experimental basis for the application of small-strain, high-stress piezoelectric materials in the active vibration control of high-stiffness heavy cantilever structures.

Many high-stiffness cantilever structures may operate in environments with varying temperature and load conditions, which pose challenges to the active vibration control performance of the BPSA. When the temperature decreases, the output performance of the BPSA declines, potentially reducing its active vibration control effectiveness. Designing a thermal insulating structure for the BPSA is an effective method to maintain its control performance in temperature-varying environments. For high-stiffness cantilever structures with loads, developing an accurate vibration control model would help maintain stable active vibration control performance. The BPSA design holds significant potential for application in the active vibration control of high-stiffness cantilever structures, and even more complex structures, across various engineering fields, including aerospace, construction, and mechanical engineering. In aerospace engineering, it can be used for vibration suppression in aircraft wings, fuselage components, and spacecraft structures, enhancing stability and performance in dynamic environments. Similarly, in construction engineering, BPSA can improve vibration control in large-span structures such as bridges and steel structures, thereby enhancing safety and durability. In mechanical engineering, BPSA can play a crucial role in stabilizing high-precision machinery and robotic arms, where vibration control is critical for maintaining accuracy and efficiency. The BPSA is well-suited for active vibration control in high-stiffness cantilever structures, but it requires the controlled structure to have a certain thickness or the shape variations of the controlled structure should not affect its operation. Further research should be carried out on how to use the characteristics which are small-strain and high-stress of piezoelectric materials to suppress the vibration for high-stiffness, high-precision and large size engineering structures.

Declaration of interest statement

We declare that we do not have any commercial or associative interest that represents a conflict of interest in connection with the work submitted.

Disclosure statement

No potential conflict of interest was reported by the author(s).

Funding

This work is supported by the National Natural Science Foundation of China (Grant No. 12272113).

ORCID

Yanju Liu http://orcid.org/0000-0001-8269-1594
Jinsong Leng http://orcid.org/0000-0001-5098-9871

References

[1] Z.K. Li, M. A. El-Meligy, and E.A. Nasr, Guided wave propagation in a high-speed rotating concrete shell reinforced by advanced nanocomposites, Mech. Adv. Mater. Struct., pp. 1–15, Jul. 2024. DOI: 10.1080/15376494.2024.2386393.

[2] Z.C. Huang, F. Huang, X.G. Wang, and F.L. Chu, Active vibration control of composite cantilever beams, Materials., vol. 16, no. 1, pp. 95, Jan. 2022. DOI: 10.3390/ma16010095.

[3] Y.G. Wang, Z. Kang, and X.P. Zhang, A velocity field level set method for topology optimization of piezoelectric layer on the plate with active vibration control, Mech. Adv. Mater. Struct., vol. 30, no. 7, pp. 1326–1339, Apr. 2023. DOI: 10.1080/15376494.2022.2030444.

[4] H.N. Song, X.B. Shan, R.R. Li, and C.W. Hou, Review on the vibration suppression of cantilever beam through piezoelectric materials, Adv. Eng. Mater., vol. 24, no. 11, pp. 12, Nov 2022. DOI: 10.1002/adem.202200408.

[5] Y.W. Zhang, S. Hou, Z. Zhang, J. Zang, Z.Y. Ni, Y.Y. Teng, and L.Q. Chen, Nonlinear vibration absorption of laminated composite beams in complex environment, Nonlinear Dyn., vol. 99, no. 4, pp. 2605–2622, Mar. 2020. DOI: 10.1007/s11071-019-05442-3.

[6] M.Y. Cui, H.Z. Liu, H.L. Jiang, Y.B. Zheng, X. Wang, and W. Liu, Active vibration optimal control of piezoelectric cantilever beam with uncertainties, Meas. Control., vol. 55, no. 5–6, pp. 359–369, May 2022. DOI: 10.1177/00202940221091244.

[7] J. Shen, W. Sun, K.P. Xu, and H. Zhang, Vibration suppression of the Blisk based on intentional mistuning of piezoelectric shunt damping patches, Mech. Adv. Mater. Struct., vol. 31, no. 26, pp. 7870–7886, Nov. 2024. DOI: 10.1080/15376494.2023.2251193.

[8] H.A. Song, X.B. Shan, W.J. Hou, C. Wang, and C.S. Han, An efficient vibration suppression technology of piezoelectric cantilever beam based on the NARX neural network, Mech. Adv. Mater. Struct., vol. 31, no. 21, pp. 5156–5163, Nov. 2024. DOI: 10.1080/15376494.2023.2212020.

[9] J. Tuma, R. Strambersky, and V. Pavelka, Modeling the use of the patch piezo-actuators for active vibration control, 22nd International Carpathian Control Conference (ICCC), May 2021. DOI: 10.1109/ICCC51557.2021.9454636.

[10] R. Rimašauskienė, A. Raza, and S. Mahato, Actuation performance of macro fibre composite (MFC) as actuator in vibration reduction of cantilever beams, Mech., vol. 29, no. 1, pp. 42–50, Feb. 2023. DOI: 10.5755/j02.mech.31732.

[11] C. Hameury, G. Ferrari, A. Buabdulla, T.M.P. Silva, P. Balasubramanian, G. Franchini, and M. Amabili, Multiple-input multiple-output active vibration control of a composite sandwich beam by fractional order positive position feedback, Mech. Syst. Sig. Process., vol. 200, pp. 110633, Oct. 2023. DOI: 10.1016/j.ymssp.2023.110633.

[12] R. Song, X.B. Shan, F.C. Lv, and T. Xie, A study of vortex-induced energy harvesting from water using PZT piezoelectric

cantilever with cylindrical extension, Ceram. Int., vol. 41, pp. S768–S773, Nov. 2015. DOI: 10.1016/j.ceramint.2015.03.262.

[13] L. Zhang, P.Y. Gao, D.X. Li, and X. Wang, Vibration characteristics and its active control of smart functionally graded circular cylindrical panels in thermal environments, Mech. Adv. Mater. Struct., vol. 21, no. 5, pp. 362–375, Jan. 2014. DOI: 10.1080/15376494.2012.697598.

[14] J.A. Moreira, F. Moleiro, A.L. Araújo, and A. Pagani, Analytical modeling of panel flutter and active control in supersonic variable stiffness composite laminates, Mech. Adv. Mater. Struct., vol. 30, no. 5, pp. 930–944, Mar. 2023. DOI: 10.1080/15376494.2022.2144970.

[15] M.P.B. de Noyer, and S.V. Hanagud, Aiaa, Modal analysis and optimization of the offset piezoceramic stack actuator, 41st Structures, Structural Dynamics, and Materials Conference, pp. 328–338, Apr. 2000. DOI: 10.2514/6.2000-1792.

[16] H.A. Song, R.R. Li, C.W. Hou, and X.B. Shan, A Low-frequency piezoelectric actuator for cantilever beams: design, modeling, and experimental evaluation, IEEE Trans. Instrum. Meas., vol. 72, pp. 1–8, 2023. DOI: 10.1109/TIM.2023.3318743.

[17] F. Callipari, M. Sabatini, F. Angeletti, P. Iannelli, and P. Gasbarri, Active vibration control of large space structures: modelling and experimental testing of offset piezoelectric stack actuators, Acta Astronaut., vol. 198, pp. 733–745, Sep 2022. DOI: 10.1016/j.actaastro.2022.05.058.

[18] M.D. Zhou, W. Liu, Z. Yao, Z.Q. Wen, L.L. Tang, B. Liang, X. Li, and Z.Y. Jia, Active vibration suppression of the cantilever sting for wind tunnel models with piezoelectric control, AIM., pp. 1323–1328, Jul. 2019. DOI: 10.1109/AIM.2019.8868557.

[19] Y. Jin, C. Qi, H. Tian, S. Dai, X. Wang, H. Ning, and D. Jiang, Optimal design of a novel nested metamaterial with hybrid auxetic-locally resonant band gap for suppressing robotic grinding vibration, Mech. Adv. Mater. Struct., pp. 1–12, Dec. 2024. DOI: 10.1080/15376494.2024.2441980.

[20] J. Rocha, P. Moniz, and A. Suleman, Aeroelastic control of a wing with active skins using piezoelectric patches, Mech. Adv. Mater. Struct., vol. 14, no. 1, pp. 23–32, Jan 2007. DOI: 10.1080/15376490600864505.

[21] A. Hashemi, J. Jang, and S. Hosseini-Hashemi, Smart active vibration control system of a rotary structure using piezoelectric materials, Sensors., vol. 22, no. 15, pp. 5691, pp. Aug 2022. DOI: 10.3390/s22155691.

[22] C.R. Vindigni, and C. Orlando, Simple adaptive V-stack piezoelectric based airfoil flutter suppression system, J. Vib. Control., vol. 29, no. 11-12, pp. 2802–2816, Jun 2023. DOI: 10.1177/10775463221085854.

[23] S.L. Cheng, X.D. Li, J.Y. Li, Y.J. Xin, Y.T. Sun, Q. Ding, Q. Yan, and H. Yan, Analysis of the low-frequency vibration attenuation capability of a novel thin-plate acoustic metamaterial, Mech. Adv. Mater. Struct., pp. 1–18, Dec 2024. DOI: 10.1080/15376494.2024.2445796.

[24] H. Zhang, W. Sun, H.T. Luo, J. Shen, and R.F. Zhang, A method of layout optimization for MFC actuators in active vibration control of composite laminates, Appl. Acoust., vol. 220, pp. 109961, Apr 2024. DOI: 10.1016/j.apacoust.2024.109961.

[25] S.P. Sun, C.Y. Zhao, and D.Q. Cao, Traveling wave vibration control of rotating functionally graded conical shells via piezoelectric sensor/actuator pairs, Arch. Appl. Mech., vol. 94, Jul no. 10, pp. 2769–2791, 2024. DOI: 10.1007/s00419-024-02614-5.

[26] J.Y. Hu, M. Wallin, M. Ristinmaa, Y. Liu, and S.T. Liu, Integrated multi-material and multi-scale optimization of compliant structure with embedded movable piezoelectric actuators, Comput. Methods Appl. Mech. Eng., vol. 421, pp. 116786, Mar 2024. DOI: 10.1016/j.cma.2024.116786.

[27] H. Zheng, G.Z. Zhao, W.F. Han, Y. Yu, and W.Z. Chen, Concurrent optimization of actuator/sensor layout and control parameter on piezoelectric curved shells with active vibration control for minimizing transient noise, Struct. Multidisc. Optim., vol. 67, no. 1, Jan 2024. DOI: 10.1007/s00158-023-03707-5.

[28] K. Bendine, Y.-J. Wei, X. Wang, M. Chen, and S.-Q. Zhang, An improved active damping of fan blade using piezoelectric MFC actuators and PSO optimization, Mech. Adv. Mater. Struct., vol. 31, no. 28, pp. 10614–10623, Dec 2024. DOI: 10.1080/15376494.2023.2294162.

[29] J.H. Zhu, J.N. Yang, W.H. Zhang, X.J. Gu, and H. Zhou, Design and applications of morphing aircraft and their structures, Front. Mech. Eng., vol. 18, no. 3, pp. Sep 2023. DOI: 10.1007/s11465-023-0750-6.

[30] I. Bruant, L. Gallimard, and S. Nikoukar, Optimization of piezoelectric sensors location and number using a genetic algorithm, Mech. Adv. Mater. Struct., vol. 18, no. 7, pp. 469–475, Sep 2011. DOI: 10.1080/15376494.2011.604600.

[31] P.P. Lu, P. Wang, and J. Lu, Decentralized vibration control of smart constrained layer damping plate, J. Vib. Control., vol. 27, no. 5-6, pp. 529–542, Mar 2021. DOI: 10.1177/1077546320931648.

[32] M.M. Jovanović, A.M. Simonović, N.D. Zorić, N.S. Lukić, S.N. Stupar, A.S. Petrović, and L. Wei, Experimental investigation of spillover effect in system of active vibration control, FME Trans., vol. 42, no. 4, pp. 329–334, Dec 2014. DOI: 10.5937/fmet1404329j.

[33] F. Ripamonti, A. Giampà, R. Giona, L. Liu, and R. Corradi, Numerical and experimental study of an active control logic for modifying the acoustic performance of single-layer panels, J. Sound Vib., vol. 520, pp. 116608, Mar. 2022. DOI: 10.1016/j.jsv.2021.116608.

[34] H. Zhang, W. Sun, H.T. Luo, and R.F. Zhang, Active vibration control of composite laminates with MFC based on PID-LQR hybrid controller, Mech. Adv. Mater. Struct., vol. 31, no. 25, pp. 6382–6399, Nov 2024. DOI: 10.1080/15376494.2023.2229841.

[35] D. Chhabra, G. Bhushan, and P. Chandna, Optimal placement of piezoelectric actuators on plate structures for active vibration control via modified controlmatrix and singular value decomposition approach using modified heuristic genetic algorithm, Mech. Adv. Mater. Struct., vol. 23, no. 3, pp. 272–280, Oct 2016. DOI: 10.1080/15376494.2014.949932.

[36] Y.F. Lu, M. Amabili, J. Wang, F. Yang, H.H. Yue, Y. Xu, and H. Tzou, Active vibration control of a polyvinylidene fluoride laminated membrane plate mirror, J. Vib. Control., vol. 25, no. 19-20, pp. 2611–2626, Oct 2019. DOI: 10.1177/1077546319862445.

[37] K.K. Afshar, and A. Javadi, Mass estimation and adaptive output feedback control of nonlinear electromagnetic levitation system, J. Sound Vib., vol. 495, pp. 115923, Mar 2021. DOI: 10.1016/j.jsv.2020.115923.

[38] D.X. Zhu, and N. Cui, Design of intelligent control for flexible linear double inverted pendulum based on particle swarm optimization algorithm, Syst, Sci. Control Eng., vol. 12, no. 1, Dec 2024. DOI: 10.1080/21642583.2024.2332409.

[39] W.G. Li, Z.C. Yang, K. Li, and W. Wang, Hybrid feedback PID-FxLMS algorithm for active vibration control of cantilever beam with piezoelectric stack actuator, J. Sound Vib., vol. 509, pp. 116243, Sep. 2021. DOI: 10.1016/j.jsv.2021.116243.

[40] V. Gupta, M. Sharma, and N. Thakur, Optimization criteria for optimal placement of piezoelectric sensors and actuators on a smart structure: a technical review, J. Intell. Mater. Syst. Struct., vol. 21, no. 12, pp. 1227–1243, Aug. 2010. DOI: 10.1177/1045389X10381659.